Joint PEV Charging Network and Distributed PV Generation Planning Based on Accelerated Generalized Benders Decomposition

Hongcai Zhang, *Member, IEEE,* Scott J. Moura, *Member, IEEE,* Zechun Hu, *Senior Member, IEEE,* Wei Qi, and Yonghua Song, *Fellow, IEEE*

***Abstract*—Integration of plug-in electric vehicles (PEVs) with distributed renewable power sources will reduce PEVs' well-to-wheels greenhouse gas emissions, promote renewable power adoption and defer power system investments. This paper proposes a multidisciplinary approach to jointly planning PEV charging stations and distributed photovoltaic (PV) power plants on a coupled transportation and power network. We formulate a two-stage stochastic programming model to determine the sites and sizes of 1) PEV charging stations; and 2) PV power plants. This proposed method incorporates comprehensive models of 1) transportation networks with explicit PEV driving range constraints; 2) PEV charging stations with probabilistic quality of service constraints; 3) PV power generation with reactive power control; and 4) alternating current distribution power flow. The formulation results in a mixed integer second order cone program. We then design a Generalized Benders Decomposition Algorithm to efficiently solve it. Numerical experiments show that investing in distributed PV power plants with PEV charging stations has multiple benefits, e.g., reducing social costs, promoting renewable power integration, alleviating power congestion. The benefits become more prominent when utilizing PV generation with reactive power control, which can also help enhance power supply quality.**

***Index Terms*—Electric vehicle, charging station, PV generation, second order cone programming, Benders Decomposition.**

NOMENCLATURE

Indices/Sets

ω/Ω	Index/set of scenarios, $\omega \in \Omega$.
d_q/o_q	The destination/origin node of path q.
$h/\mathcal{H}_q$	Index/set of sub-paths on path q, $h \in \mathcal{H}_q$.
$i/\mathcal{I}$	Index/set of transportation nodes, $i \in \mathcal{I}$. $\mathcal{I}_m \subseteq \mathcal{I}$ is the set of transportation nodes whose electricity are supplied by distribution bus m.
$(i,j)/\mathcal{A}$	Index/set of transportation arcs, $(i,j) \in \mathcal{A}$.
$k/\mathcal{K}$	Index/set of PEV types, $k \in \mathcal{K}$.
$m/\mathcal{M}$	Index/set of buses of the distribution network, $m \in \mathcal{M}$. For the substation bus (root bus), $m = 0$. $\mathcal{M}_+ = \mathcal{M} \setminus \{0\}$. $\mathcal{M}_m \subset \mathcal{M}$ is the set of buses that are connected to bus m and bus m lies between them and root bus 0.
$(m,n)/\mathcal{B}$	Index/set of lines of the distribution network, $(m,n) \in \mathcal{B}$. On line (m,n), bus n lies between buses m and 0.
$q/\mathcal{Q}$	Index/set of paths, $q \in \mathcal{Q}$. $\mathcal{Q}_i \subseteq \mathcal{Q}$ is the set of paths through transportation node i.
t	Index of time intervals.

Parameters

α	Service level of charging stations.
$\lambda_{q,k}$	Volume of type k PEV traffic demand on path q, in h^{-1}. $\lambda_{q,k,\omega t}$ is $\lambda_{q,k}$ during time interval t in scenario ω.
π_ω	Probability of scenario ω, in %.
$\xi_{m,\omega t}$	Per unit PV power output at distribution bus m during time interval t in scenario ω.
ζ	The capital recovery factor.
Δt	Time interval, one hour in this paper.
c_1	Fixed cost for building a new charging station at transportation node i, in \$.
c_2	Cost for adding an extra charging spot in a charging station at transportation node i, in \$.
c_3	Fixed cost for building a PV power plant at distribution bus m, in \$.
c_4	Cost for adding extra PV panels at distribution bus m, in \$/kVA.
$c_{\mathrm{e}}^+/c_{\mathrm{e}}^-$	Per-unit cost for energy purchase/selling of the whole distribution system at rood bus 0, in \$/kWh.
c_{p}	Per-unit penalty cost for unsatisfied PEV charging power, in \$/kWh.
$\overline{I_{mn}}$	Upper limit of the branch current of distribution line (m,n), in kA.
N^{pv}	Maximum number of PV power plants.
p^{sp}	Rated charging power of a PEV charging spot, in kW.
$s^{\mathrm{b}}_{m,\omega t}$	Apparent base load at distribution bus m, in kVA.

This work was supported in part by the National Natural Science Foundation of China (51477082) and State Grid Corporation of China (52110417001G). A preliminary version of this paper was presented at the 2017 IEEE Power and Energy Society General Meeting, Chicago, IL, USA, 2017. Corresponding author: Zechun Hu.

H. Zhang was with the Department of Electrical Engineering, Tsinghua University, Beijing, 100084, China when this work was conducted. He is now with the Department of Civil and Environmental Engineering, University of California, Berkeley, California, 94720, USA (email: zhang-hc13@berkeley.edu).

S. J. Moura is with the Department of Civil and Environmental Engineering, University of California, Berkeley, California, 94720, USA, and also with the Smart Grid and Renewable Energy Laboratory, Tsinghua-Berkeley Shenzhen Institute, Shenzhen, 518055, China (email: smoura@berkeley.edu).

Z. Hu is with the Department of Electrical Engineering, Tsinghua University, Beijing, 100084, China (email: zechhu@tsinghua.edu.cn).

W. Qi is with the Desautels Faculty of Management, McGill University, Montreal, Quebec, Canada H3A 1G5 (email: wei.qi@mcgill.ca).

Y. Song is with the Department of Electrical and Computer Engineering, University of Macau, Macau, China and also with the Department of Electrical Engineering, Tsinghua University, Beijing, 100084, China (email: yhsong@tsinghua.edu.cn).

$\overline{S^{\text{pv}}}$ Maximum total PV power generation capacity in the system, in kVA.

T_k Charging time requirement for type k PEVs.

v_0 Square of the nodal voltage magnitude at root bus 0.

$\underline{V_m}/\overline{V_m}$ Lower/upper limit of nodal voltage at distribution bus m, in kV.

$\overline{y_m^{\text{pv}}}$ Maximum PV power capacity at distribution bus m, in kVA.

z_{mn} Impedance of distribution line (m,n), in ohm. z_{mn}^* is its conjugate.

Decision variables (first-stage, X)

$\gamma_{q,k,i}$ Binary charge choice of type k PEVs on path q at transportation node i: $\gamma_{q,k,i}=1$, if they get charged; $\gamma_{q,k,i}=0$, otherwise.

x_i^{cs} Binary charging station location decision at transportation node i: $x_i^{\text{cs}}=1$, if there is a station at transportation node i; $x_i^{\text{cs}}=0$, otherwise.

x_m^{pv} Binary PV generation location decision at distribution bus m: $x_m^{\text{pv}}=1$, if there is PV at distribution bus m; $x_m^{\text{pv}}=0$, otherwise.

y_i^{cs} Integer number of charging spots at transportation node i.

y_m^{pv} Invested capacity (maximum nameplate apparent power) of PV panels at distribution bus m, in kVA.

Decision variables (second-stage, $Y_{\omega t}$)

$\lambda_{k,i}$ Volume of type k PEVs that require charging at node i, in h^{-1}. $\lambda_{k,i,\omega t}$ is $\lambda_{k,i}$ during t in scenario ω.

$l_{mn,\omega t}$ Square of the magnitude of distribution line (m,n)'s apparent current during t in scenario ω, in kA^2.

$p_{i,\omega t}^{\text{ev}}$ Active PEV charging power at node i during t in scenario ω, in kW.

$p_{0,\omega t}^{+/-}$ Total purchasing/selling power at root bus 0 during t in scenario ω, in kW. $p_{0,\omega t}=p_{0,\omega t}^{+}-p_{0,\omega t}^{-}$.

$p_{m,\omega t}$ Total active power injection at bus m during t in scenario ω, in kW.

$p_{m,\omega t}^{\text{loss}}$ Unsatisfied PEV charging demands at bus m during t in scenario ω, in kW.

$s_{m,\omega t}$ Total apparent power injection at bus m during t in scenario ω, in kVA. $s_{m,\omega t}=p_{m,\omega t}+jq_{m,\omega t}$. $s_{0,\omega t}$ (at bus 0) is also the power consumption of the whole distribution system.

$s_{m,\omega t}^{\text{ev}}$ Apparent PEV power at bus m during t in scenario ω, in kVA.

$S_{mn,\omega t}$ Apparent power flow from bus m to bus n during t in scenario ω, in kVA.

$v_{m,\omega t}$ Square of nodal voltage at bus m during t in scenario ω, in kV.

I. Introduction

Integration of PEVs with distributed renewable resources can help reduce PEVs' well-to-wheel greenhouse gas emissions, promote renewable power adoption, alleviate power congestion and defer power system investment.

Facilitating PEVs to consume low-emission renewable power is one of the key approaches to decarbonizing our transportation systems. The emissions of PEVs depend on their energy supply mix. PEVs in areas with high penetration of coal-fired plants may emit more than traditional electric-gasoline hybrid vehicles or even internal combustion engine vehicles [1]. Integrating PEVs with renewable power resources, e.g., wind and photovoltaic (PV) power etc., can help fully realize PEVs' emission reduction potential whilst promoting renewable power adoption.

Building PEV charging infrastructure along with distributed renewable power generation can also alleviate power congestion, and thereafter, defer power system investments. Rapidly growing PEV charging demands may threaten secure operation of power distribution networks. For *destination charging*, coordinated controlling or vehicle-to-grid technologies can be utilized to alleviate PEV charging power's negative effect, while uncontrollable *fast-charging* power may cause significant power congestion.[1] Considering that upgrading distribution systems is usually expensive, installing cheap distributed renewable generation to satisfy congested PEV load is a promising solution.

The growing PEV population is leading to massive investments in charging infrastructure recently. In China, 4.8 million distributed charging spots and more than twelve thousand fast-charging stations are planned for construction by 2020 [2]. This investment boom provides an opportunity to integrate PEVs with renewable resources at the planning stage, i.e., jointly plan PEV charging stations with distributed renewable resources, so that we can more effectively reap the aforementioned benefits.

Integrating renewable power with PEV charging stations has been a research hotspot over recent years. Most of the published papers focus on economic benefit evaluation or coordinated control strategies. Takagi et al. [3] adopted PEV battery-swapping stations to accommodate PV power. MacHiels et al. [4] studied the economic benefit of integrating PV generation with fast-charging stations. Brenna et al. [5], Liao et al. [6], and Wu et al. [7] demonstrated that coordinated PEV charging could significantly improve distributed PV power integration. Alam et al. [8] showed that coordinated PEV charging could alleviate voltage rise problems caused by PV power injection.

Some papers studied the sizing problem of PEV charging stations whose electricity is partly or totally supplied by renewable power generation. Liu et al. [9] studied joint capacity planning of on-site PV generation and battery-swapping stations. Mouli et al. [10] designed a workplace PEV charging station powered by PV generation with vehicle-to-grid technology. Quoc et al. [11] studied the sizing of a PEV charging station powered by commercial grid-integrated PV systems considering reactive power support. Ugirumurera et al. [12] studied the sizing of a PEV charging station whose electricity is supplied completely from PV power generation. Zhang et al.

[1]This will particularly be the case in highway transportation networks on intercity corridors, where the covered areas are mostly rural and base loads are low with weak power systems.

[13] developed a stochastic programming approach to jointly size PEV chargers, PV panels and battery storage system in one charging station.

Few published papers have studied the joint sizing and siting problem of PEV charging stations and renewable power generation. Shaaban et al. [14] proposed a multi-year multi-objective planning algorithm for uncoordinated PEV parking lots and renewable generation. Moradi et al. [15] developed a multi-objective model to optimize the sites and sizes of charging stations and distributed renewable generation. Amini et al. [16] proposed a two-stage approach to simultaneously allocating PEV charging stations with distributed renewable resources in distribution systems. Kasturi et al. [17] and Erdinç et al. [18] developed planning models to jointly optimize the sites and sizes of PEV charging stations, PV power plants, and energy storage systems in distribution systems considering future energy management controlling. Quevedo et al. [19] developed a multi-stage distribution expansion planning model which also jointly optimizes investments in PEV charging stations, renewable power generation and energy storage systems. Most of the above papers, e.g., [14]–[17], adopted heuristic algorithms to solve their planning problems, which cannot ensure optimality of solutions. Furthermore, in practice, PEVs' charging power is impacted by their mobility behavior in transportation networks. However, all of the above papers only consider destination charging demands and do not explicitly incorporate transportation network models.

This paper focuses on joint planning of PEV fast-charging stations and distributed PV power plants. We advance this research by developing a novel integrated planning model to jointly determine the sites and sizes of 1) PEV fast-charging stations; 2) PV power plants on a coupled transportation and power network. The innovations of the proposed method compared with the aforementioned literature are threefold:

1) The PEV traffic flows and charging demands are explicitly modeled on a transportation network by the modified capacitated-flow refueling location model (CFRLM) under PEV driving range constraints.
2) This paper considers the new PV power plants with reactive power control so that they can help enhance distribution system reliability. Furthermore, we use the second order cone programming (SOCP) to describe the power constraints of PV inverters so that both the active and reactive power can be accurately optimized. In contrast, the aforementioned literature does not consider reactive power control.
3) The proposed planning model is a two stage stochastic mixed-integer SOCP (MISOCP), which can be solved by off-the-shelf solvers and the optimality of the solution can be guaranteed. Furthermore, we also adopt an Accelerated Generalized Benders Decomposition Algorithm to expedite the computation in large scale scenarios. We prove that the algorithm will converge to the optimal solution after a finite number of iterations. To the best of our knowledge, Benders Decomposition Algorithms are widely applied for power scheduling [20]–[22], unit commitment [23], [24], power system planing [25] etc., but are not used in joint PEV charging station and PV power plant planning in published literature.

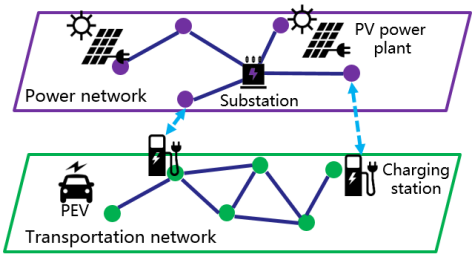

Fig. 1. A coupled transportation and power network.

To the best of our knowledge, this is the first time that an MISOCP planning model with explicit transportation and power network constraints is developed for joint planing of PEV charging stations and PV power plants. This is also the first time that the Accelerated Benders Decomposition Algorithm is developed for the planning. Numerical experiments are conducted to illustrate the effectiveness of the proposed method. The benefits of the joint planning of charging stations with PV power plants and the adoption of PV reactive power control are discussed.

Section II formulates the two-stage stochastic MISOCP planning model. The models of transportation networks, PEV charging stations, and PV power generation are also introduced. In Section III, the Accelerated Generalized Benders Decomposition Algorithm is given. Case studies are described in Section IV and Section V concludes the paper.

II. Joint Planning Model

A. Problem Statement and Major Notations

This paper studies the joint PEV charging station and PV generation planning problem in a transportation network coupled with a high-voltage distribution network (as illustrated in Fig. 1). We assume the planner is a social planner and has access to parameters of both the transportation and power systems. It needs to optimize: 1) the sites and sizes of PEV charging stations in the transportation network; and 2) the sites and sizes of PV power plants in the high voltage distribution network. Its objective is to minimize the social costs of the whole coupled system, including the investment costs for PEV charging stations and PV power plants, and the operation costs for purchasing electricity etc. The planning result should fulfill the expected PEV charging demands and satisfy the power network's security operation constraints. We assume that the system can purchase electricity from and sell surplus electricity (at a lower price) to the upper-level power grid.

We assume that future PEVs are composed by a set of PEV types, $\mathcal{K}$, with different driving ranges (battery capacities). Considering heterogeneous PEV parameters instead of assuming homogeneous PEVs (as in references [9]–[12], [14]–[16]) allows us to more realistically model future PEVs' charging behaviors.

Notations. We use a directed graph $G(\mathcal{I}, \mathcal{A})$ to model the transportation network, where $\mathcal{I}$ denotes the node set and $\mathcal{A}$ denotes the arc set. A *node* $i \in \mathcal{I}$ is a candidate charging station location, and an *arc* $(i, j) \in \mathcal{A}$ is the road link between

two adjacent nodes, i and j. The route that a PEV drives from an origin node to the corresponding destination node is called a *path* $q \in \mathcal{Q}$; and a segment of a path q is its *sub-path* $h \in \mathcal{H}_q$. We apply tuples $(o_q, d_q, \lambda_{q,k})$, $\forall q \in \mathcal{Q}$, $\forall k \in \mathcal{K}$, to describe PEV traveling demands, in which $\lambda_{q,k}$ represents the Poisson volume of traffic flow from origin node o_q to destination node d_q on path q of type k PEVs. We use a directed graph $G(\mathcal{M}, \mathcal{B})$ to model the power distribution network, where $\mathcal{M}$ denotes the distribution bus set and $\mathcal{B}$ denotes the distribution line set. The root bus is indexed by 0. We let $\mathcal{M}_+ = \mathcal{M} \setminus \{0\}$. A bus $m \in \mathcal{M}_+$ is a candidate location for building PV power plants. The distribution line between two adjacent buses m and n (n lies between bus m and root bus 0) is indexed by $(m, n) \in \mathcal{B}$. We use $\mathcal{I}_m$ to denote the set of transportation nodes whose electricity is supplied by distribution bus m.

The investment decision variables are denoted by $X = \{x_i^{\text{cs}}, y_i^{\text{cs}}, x_m^{\text{pv}}, y_m^{\text{pv}}\}$. $x_i^{\text{cs}} \in \{0, 1\}$ is a binary PEV charging station location decision at node i: $x_i^{\text{cs}} = 1$, if there is a station at node i; $x_i^{\text{cs}} = 0$, otherwise. $y_i^{\text{cs}} \in \mathbb{Z}$ is the number of charging spots at location i. $x_m^{\text{pv}} \in \{0, 1\}$ is a binary PV power plant location decision at distribution bus m: $x_m^{\text{pv}} = 1$, if there is a plant; $x_m^{\text{pv}} = 0$, otherwise. $y_m^{\text{pv}} \in \mathbb{R}$ is the capacity of the PV power plant at bus m.

The probabilistic PEV charging demands and PV generation are crucial stochastic inputs that will affect the planning result's actual performance. Hence, we generate a finite set of potential scenarios (Ω), i.e., hourly typical base load, traffic flow and PV generation curves, to represent the future probabilistic situations for planning. Each scenario $\omega \in \Omega$ has an occurrence probability π_ω. With these scenarios, we can evaluate the planning result's future operation performance on an hourly basis. Hereafter, we use index ωt to denote the operation variables or parameters in hour t of scenario ω.

B. Planning Objective

We formulate a two-stage stochastic programming for the planning. Its objective includes the equivalent annual investment costs and the weighted average annual operation costs for all the future scenarios, as follows:

$$J = \min_{X} \left\{ C^{\text{I}}(X) + \sum_{\omega \in \Omega} \pi_\omega C^{\text{O}}(X, \omega) \right\}. \tag{1}$$

The first-stage equivalent annual investment cost is:

$$C^{\text{I}}(X) = \zeta \sum_{i \in \mathcal{I}} \left(c_1 x_i^{\text{cs}} + c_2 y_i^{\text{cs}}\right) + \zeta \sum_{m \in \mathcal{M}_+} \left(c_3 x_m^{\text{pv}} + c_4 y_m^{\text{pv}}\right), \tag{2}$$

where, c_1 and c_3 are the fixed costs for building one PEV charging station and a PV power plant, respectively; c_2 and c_3 are the variable costs for adding an extra charging spot and per-unit PV panel, respectively. ζ is the capital recovery factor, which converts the present investment costs into a stream of equal annual payments over the planning horizon. The first two terms of (2) represent the fixed cost of building PEV charging stations and the variable cost in proportion with the number of charging spots. The last two terms represent the fixed cost per PV power plant and the cost per kVA PV panels.

The second stage annual operation costs given the investment decision X for each scenario ω is:

$$\begin{aligned} C^{\text{O}}(X, \omega) = \min_{Y_{\omega t}} \Bigg\{ & 365 \sum_t \left(c_{\text{e}}^+ p_{0,\omega t}^+ \Delta t - c_{\text{e}}^- p_{0,\omega t}^- \Delta t\right) \\ & + 365 \sum_t \sum_{m \in \mathcal{M}_+} \left(c_{\text{p}} p_{m,\omega t}^{\text{loss}} \Delta t\right) \\ & + 365 \sum_t \sum_{m \in \mathcal{M}_+} \sigma \left| v_{m,\omega t} - v_0 \right| \Bigg\}, \end{aligned} \tag{3}$$

where, $Y_{\omega t}$ is the second stage optimization variable including the nodal voltages, line currents, PEV charging power, PV generation etc. in each hour t of each scenario ω. The first two terms in (3) are the system's annual expected energy costs, i.e., the costs for purchasing electricity minus the income by selling surplus electricity. $p_{0,\omega t}^+$ and $p_{0,\omega t}^-$ are the purchasing and selling power, respectively; c_{e}^+ and c_{e}^- are the corresponding per-unit price.[2] The third term is the penalty for unsatisfied PEV charging demand, $p_{m,\omega t}^{\text{loss}}$; c_{p} is the corresponding per-unit cost. The fourth term is the penalty for undesirable voltage deviations.[3] $v_{m,\omega t}$ and v_0 are the square of nodal voltage magnitude at bus m and root bus 0, respectively. Coefficient σ is used to balance it with the first two monetary objectives.[4]

C. Transportation Network Constraints

Given the traffic flows $(o_q, d_q, \lambda_{q,k})$, $\forall q \in \mathcal{Q}$, $\forall k \in \mathcal{K}$, we utilize the modified CFRLM [26], [27] to explicitly model PEVs' driving range constraints in the transportation network. This model requires that *any sub-path with a distance longer than a PEV's driving range should cover at least one charging station* so that the PEVs can travel through that sub-path with adequate charging service. Obviously, this model defines the feasible set of a PEV's charging locations in a path.

For completeness, we briefly introduces the CFRLM by the illustrative transportation network in Fig. 2. We assume a PEV with its battery fully charged (with 100 km driving range, for example) leaves at origin node o and needs to arrive at destination node d. It may get charged on any of the candidate charging station locations, $\mathcal{I} \setminus \{o, d\}$. The path $q = o123456d$ excluding nodes o and d can be divided into three sub-paths whose length are longer than the PEV's driving range, i.e., $\mathcal{H}_q = \{1234, 2345, 3456\}$. Hence, on each sub-path in $\mathcal{H}_q$, the PEV should get charged for at least once; otherwise, its battery may get fully depleted on road.

Considering different types of PEVs have different driving ranges, we can generate one sub-path set (denoted by $\mathcal{H}_{q,k}$) for

[2]We assume the electricity prices are static as in references [14], [15] in this paper. Our proposed model can be readily extended to consider time-varying stochastic electricity prices. For example, we can generate a number of electricity price scenarios, i.e., $c_{\text{e},\omega t}^+$ and $c_{\text{e},\omega t}^-$ (where ω indexes scenarios and t indexes time), as the input and substitute the price parameters $c_{\text{e}}^{+/-}$ in objective (3) by $c_{\text{e},\omega t}^{+/-}$.

[3]This term can be easily reformulated as an affine objective by adding two linear inequality constraints for each || (absolute value) term.

[4]In practice, σ should be designed according to the system's parameters and the power supply quality requirement. We assume it is given in this paper.

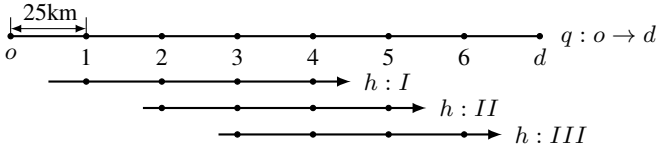

Fig. 2. An illustrative transportation network [26]. It has 8 nodes, $\mathcal{I} = \{o, 1, 2, 3, 4, 5, 6, d\}$, one OD pair, (o, d), and one path, $\mathcal{Q} = \{o123456d\}$. Every two adjacent nodes form one arc with 25 km distance.

each PEV type k on path q. Then, the driving range constraints described above can be formulated as follows:

$$\sum_{i \in \mathcal{I}_h} \gamma_{q,k,i} \geq 1, \quad \forall h \in \mathcal{H}_{q,k}, \forall q \in \mathcal{Q}, \forall k \in \mathcal{K}, \tag{4}$$

$$\gamma_{q,k,i} \leq x_i^{\text{cs}}, \quad \forall i \in \mathcal{I}, \forall q \in \mathcal{Q}, \forall k \in \mathcal{K}, \tag{5}$$

where, $\gamma_{q,k,i} \in \{0, 1\}$ is a binary variable indicating charge choice of type k PEVs on path q at node i: $\gamma_{q,k,i} = 1$, if they get charged; $\gamma_{q,k,i} = 0$, otherwise. $\mathcal{I}_h \subset \mathcal{I}$ is the set of candidate charging locations on sub-path h. Equation (4) ensures that the PEVs are charged at least once on each sub-path. Equation (5) constrains PEVs to charge at nodes with charging stations.

In a complex transportation network, the total type k PEV traffic flow charging at location i, $\lambda_{k,i}$, is composed by different traveling demands $\lambda_{q,k}$, which can be calculated as:

$$\lambda_{k,i} = \sum_{q \in \mathcal{Q}_i} \lambda_{q,k} \gamma_{q,k,i}, \quad \forall k \in \mathcal{K}, \forall i \in \mathcal{I}, \tag{6}$$

where, $\mathcal{Q}_i$ is the set of paths through node i, $\mathcal{Q}_i \subset \mathcal{Q}$.

D. Quality of Service Constraints of PEV Charging Station

Given the charging locations of PEVs determined by the above subsection, we need to optimize the number of charging spots at each location. We adopt a service level model [27] to size a charging station given heterogeneous charging demands. We assume PEVs of type $k \in \mathcal{K}$ arrive in a station at location i following a Poisson process with parameter $\lambda_{k,i}$ (given in equation (6)) and requires T_k units of charging time.

Then, to ensure a charging station's *quality of service*, i.e., *the probability that a PEV can get instantly serviced without waiting*, is beyond a designed threshold, α, the minimum installed number of charging spots, y_i^{cs}, shall be constrained by the following equation:

$$y_i^{\text{cs}} \geq \sum_{k \in \mathcal{K}} T_k \lambda_{k,i} + \Phi^{-1}(\alpha) \sqrt{\sum_{k \in \mathcal{K}} T_k \lambda_{k,i}}, \quad \forall i \in \mathcal{I}, \tag{7}$$

where, $\Phi(\cdot)$ is the cumulative distribution function of the standard normal distribution. The first term in the right-hand side of (7) is the required number of charging spots to satisfy the expected charging demands and is proportional to the Poisson arrival rate. The second term corresponds to the extra spots to satisfy any demand in excess of the mean and can be viewed as the "safety stock." In practice, higher α leads to more "safety stock" and ensures better quality of service.

Hence, by combining equations (6) and (7) to eliminate $\lambda_{k,i}$, and substituting $\gamma_{q,k,i}$ with $\gamma_{q,k,i}^2$ in the square root, we have the quality of service constraint for a charging station servicing $\mathcal{K}$ types of PEVs in a mixed-integer SOCP form, as follows:

$$y_i^{\text{cs}} \geq \max_{\forall \omega \in \Omega, \forall t} \left(\sum_{q \in \mathcal{Q}_i} \sum_{k \in \mathcal{K}} T_k \lambda_{q,k,\omega t} \gamma_{q,k,i} + \Phi^{-1}(\alpha) \sqrt{\sum_{q \in \mathcal{Q}_i} \sum_{k \in \mathcal{K}} T_k \lambda_{q,k,\omega t} \gamma_{q,k,i}^2} \right), \ \forall i \in \mathcal{I}. \tag{8}$$

This equation ensures that the quality of service constraints are satisfied for all the future scenarios.

E. Investment & Operation Constraints of PV Generation

We assume that the planner may build a PV power plant at any distribution bus in $\mathcal{M}_+$, but the installed PV capacity y_m^{pv} at each bus is bounded by an upper limit $\overline{y_m^{\text{pv}}}$, as follows:

$$0 \leq y_m^{\text{pv}} \leq \overline{y_m^{\text{pv}}} x_m^{\text{pv}}, \quad \forall m \in \mathcal{M}_+. \tag{9}$$

The planner may also need to constrain the total number and capacity of the PV power plants in the system, respectively:

$$\sum_{m \in \mathcal{M}_+} x_m^{\text{pv}} \leq N^{\text{pv}}, \tag{10}$$

$$\sum_{m \in \mathcal{M}_+} y_m^{\text{pv}} \leq \overline{S^{\text{pv}}}, \tag{11}$$

where, N^{pv} is the maximum number of PV power plants; $\overline{S^{\text{pv}}}$ is the maximum total PV power capacity in the system.

Given the nameplate PV capacity at a bus m, y_m^{pv}, the active PV power generation $p_{m,\omega t}^{\text{pv}}$ is upper-bounded by the solar irradiation (influence by both whether and time etc.). In this paper, we assume that PV generation can be curtailed. Hence, $p_{m,\omega t}^{\text{pv}}$ is constrained by the following equation:

$$0 \leq p_{m,\omega t}^{\text{pv}} \leq \xi_{m,\omega t} y_m^{\text{pv}}, \quad \forall m \in \mathcal{M}_+, \forall \omega \in \Omega, \forall t, \tag{12}$$

where, $\xi_{m,\omega t}$ is the maximum per-unit PV power output during hour t in scenario ω depending on solar radiation.

Besides active power generation, PV power plants with fast-reacting and VAR-capable inverters can also generate or consume reactive power which can help enhance security and efficiency of distribution system operations by regulating voltage [28], [29]. Since the modulus of a PV power plant's apparent power, $|s_{m,\omega t}^{\text{pv}}|$, is no larger than its nameplate capacity, a PV power plant's reactive power, $q_{m,\omega t}^{\text{pv}}$, should be constrained as follows:

$$\sqrt{|p_{m,\omega t}^{\text{pv}}|^2 + |q_{m,\omega t}^{\text{pv}}|^2} \leq y_m^{\text{pv}}, \quad \forall m \in \mathcal{M}_+, \omega \in \Omega, \forall t, \tag{13}$$

$$s_{m,\omega t}^{\text{pv}} = p_{m,\omega t}^{\text{pv}} + j q_{m,\omega t}^{\text{pv}}, \quad \forall m \in \mathcal{M}_+, \omega \in \Omega, \forall t. \tag{14}$$

Equation (13) is in the form of an SOCP. Equation (14) calculates the apparent power. In the above PV model, $q_{m,\omega t}^{\text{pv}}$ is adjustable and can be either negative or positive.

F. Power Network Constraints

For each line (m, n) of the distribution network, let $S_{mn} = P_{mn} + jQ_{mn}$, l_{mn}, and z_{mn} denote its apparent power flow, square of current magnitude, and impedance, respectively. For each bus m of the distribution network, $s_m = p_m + jq_m$ and

$v_m = |V_m|^2$ denote its nodal apparent power injection, and square of nodal voltage magnitude, respectively. $v_0 = |V_0|^2$ (at root bus 0) is fixed. $\mathcal{M}_m \subset \mathcal{M}$ is the set of buses that are connected to bus m from the opposite side of root bus 0.

Hence, the operation of the distribution system shall satisfy the alternating current power flow constraints, as follows:

$$\forall (m,n) \in \mathcal{B}, \forall \omega \in \Omega, \forall t:$$

$$S_{mn,\omega t} = s_{m,\omega t} + \sum_{u \in \mathcal{M}_m} (S_{um,\omega t} - z_{um} l_{um,\omega t}), \tag{15}$$

$$0 = s_{0,\omega t} + \sum_{u \in \mathcal{M}_0} (S_{u0,\omega t} - z_{u0} l_{u0,\omega t}), \tag{16}$$

$$v_{m,\omega t} - v_{n,\omega t} = 2\mathrm{Re}(z_{mn}^* S_{mn,\omega t}) - |z_{mn}|^2 l_{mn,\omega t}, \tag{17}$$

$$|S_{mn,\omega t}|^2 \le l_{mn,\omega t} v_{m,\omega t}, \tag{18}$$

where, z_{mn}^* is the conjugate of z_{mn} and $\mathrm{Re}(\cdot)$ denotes the real part of a complex number. In the traditional power flow model [30], equation (18) should be $|S_{mn}|^2 = l_{mn} v_m$, which is non-convex. Here, we adopt its convex SOCP relaxation [31]. Due to limited space, the detailed introduction of the power flow model is omitted in this paper but can be found in [31].

The nodal apparent power injection is calculated as follows:

$$s_{m,\omega t} = s^{\mathrm{pv}}_{m,\omega t} - s^{\mathrm{ev}}_{m,\omega t} - s^{\mathrm{b}}_{m,\omega t}, \forall m \in \mathcal{M}_+, \forall \omega \in \Omega, \forall t, \tag{19}$$

where, $s^{\mathrm{pv}}_{m,\omega t}$, $s^{\mathrm{ev}}_{m,\omega t}$, and $s^{\mathrm{b}}_{m,\omega t}$ are the PV generation, PEV charging load, and base load at bus m, respectively.

For a distribution network, the power injection at root bus 0, $s_{0,\omega t}$, is the net power consumption/generation of the whole system [31]. Its active part is the system's actual purchasing (positive) or selling (negative) electricity. We adopt the following equation to distinguish purchasing and selling electricity:[5]

$$p_{0,\omega t} = p^{+}_{0,\omega t} - p^{-}_{0,\omega t}, \quad \forall \omega \in \Omega, \forall t, \tag{20}$$

The line currents and nodal voltages of the distribution network cannot violate their permitted ranges, as follows:

$$l_{mn,\omega t} \le |\overline{I_{mn}}|^2, \quad \forall (m,n) \in \mathcal{B}, \omega \in \Omega, \forall t, \tag{21}$$

$$|\underline{V_m}|^2 \le v_{m,\omega t} \le |\overline{V_m}|^2, \quad \forall m \in \mathcal{M}_+, \omega \in \Omega, \forall t, \tag{22}$$

where, $\overline{I_{mn}}$ is the line current capacity; $\underline{V_m}/\overline{V_m}$ is the lower/upper limit of nodal voltage magnitude.[6]

G. Coupling Constraints

The transportation network and the power network are coupled together by the PEV charging stations. The hourly average PEV charging power at transportation node i is:

$$p^{\mathrm{ev}}_{i,\omega t} = p^{\mathrm{sp}} \sum_{q \in \mathcal{Q}_i} \sum_{k \in \mathcal{K}} T_k \lambda_{q,k,\omega t} \gamma_{q,k,i}, \forall i \in \mathcal{I}, \forall \omega \in \Omega, \forall t, \tag{23}$$

where, p^{sp} is the rated charging power of a charging spot.

[5]Because the selling price is lower than the purchasing price, the system will not buy and sell electricity simultaneously, which makes negative profit.

[6]Though the nodal voltage deviations are already penalized in the objective (3), it is still possible that they may be too large in heavy load scenarios which deteriorates electricity quality significantly. Hence, it is necessary to include this constraint.

The PEV charging power at distribution bus m is:

$$p^{\mathrm{ev}}_{m,\omega t} + p^{\mathrm{loss}}_{m,\omega t} = \sum_{i \in \mathcal{I}_m} p^{\mathrm{ev}}_{i,\omega t}, \quad \forall m \in \mathcal{M}_+, \forall \omega \in \Omega, \forall t, \tag{24}$$

$$p^{\mathrm{loss}}_{m,\omega t} \ge 0, \quad \forall m \in \mathcal{M}_+, \forall \omega \in \Omega, \forall t. \tag{25}$$

We assume the base load $s^{\mathrm{b}}_{m,\omega t}$ must be satisfied. However, when the charging demands grow beyond the system's service ability, part of them can be discarded, i.e., $p^{\mathrm{loss}}_{m,\omega t} \ge 0$.

The planning model (1)–(25) is an MISOCP and can be solved by off-the-shelf solvers, e.g., CPLEX [32].

III. Benders Decomposition Algorithm

A significant number of scenarios should be considered to effectively describe the stochastic inputs, i.e., hourly base load, traffic flow and PV generation curves in different weather of different days in a year. Thus, the planning model is of high dimension and computationally expensive if directly using off-the-shelf solvers. To address this challenge, we adopt the Generalized Benders Decomposition Algorithm [33].

In each scenario, the second stage operation problem solves a 24 hour dynamic optimal power flow problems. However, the corresponding decision variables, e.g., the PEV charging power and the PV generation, in adjacent hours are not coupled. Therefore, when the first stage investment decision, X, is given, the second stage operation problems in every hour of every scenario can be decoupled into low-scale sub-problems that can be efficiently solved in parallel. Based on the above analysis, the proposed algorithm naturally decouples the problem into a master problem, i.e., the planning problem, and a collection of sub-problems, i.e., the operation problem of every hour given X.

For simplicity, we reformulate the original problem (1)-(25) into its standard MISOCP form, as follows:

$$\min_{X, Y_{\omega t}} \quad c^\top X + \sum_{\omega \in \Omega} \sum_{t} d^\top_{\omega t} Y_{\omega t} \tag{26}$$

$$\text{s.t.: } \|A_{\omega tj} X + B_{\omega tj} Y_{\omega t} + e_{\omega tj}\|_2 \le c^\top_{\omega tj} X + d^\top_{\omega tj} Y_{\omega t} + f_{\omega tj}, \quad \forall \omega, \forall t, \forall j, \tag{27}$$

$$X \in \mathbb{X}, \tag{28}$$

where, wt (hour t in scenario ω) is the index of the sub-problems; j is the index of the second order cones. The objective (26) is equivalent to (1); c and $d_{\omega t}$ are its coefficient vectors. Equation (27) describes the constraints that couple the first-stage decision variables, X, and second-stage decision variables, $Y_{\omega t}$; A_{wtj}, B_{wtj}, c_{wtj}, d_{wtj}, e_{wtj} and f_{wtj} are the corresponding coefficient matrices or vectors. Equation (28) describes other constraints that are only relevant to first-stage decision variables, X; $\mathbb{X}$ is the feasible set of X that is uniform across sub-problems. Note that parts of X are integer variables, which makes the problem hard to scale.

Given a fixed first stage solution $\hat{X}$, the sub-problem ωt is a convex SOCP (all the variables are continuous):

$$\min_{Y_{\omega t}} \quad d^\top_{\omega t} Y_{\omega t} \tag{29}$$

$$\text{s.t.: } \|B_{\omega tj} Y_{\omega t} + A_{\omega tj} \hat{X} + e_{\omega tj}\|_2 \le d^\top_{\omega tj} Y_{\omega t} + c^\top_{\omega tj} \hat{X} + f_{\omega tj}, \quad \forall j. \tag{30}$$

Then, we can obtain the sub-problem's dual problem [34]:

$$\max_{\mu_{\omega tj},u_{\omega tj},\forall j} \quad \Big\{ \sum_j -u_{\omega tj}^\top \left(A_{\omega tj}\hat{X} + e_{\omega tj}\right) - \mu_{\omega tj}\left(c_{\omega tj}^\top \hat{X} + f_{\omega tj}\right) \Big\} \tag{31}$$

$$\text{s.t.: } \sum_j \left(B_{\omega tj}^\top u_{\omega tj} + \mu_{\omega tj} d_{\omega tj}\right) = d_{\omega t}, \tag{32}$$

$$\|u_{\omega tj}\|_2 \le \mu_{\omega tj}, \qquad \forall j, \tag{33}$$

in which, $\mu_{\omega tj}$ and $u_{\omega tj}$ are the vectors of dual variables. The complete formulation for the subproblem and the derivation for its dual problem are given in Appendix A. The corresponding master problem is:

$$\min_{X,z} \quad c^\top X + z \tag{34}$$

$$\text{s.t.: } z \ge \sum_{\omega\in\Omega}\sum_t\sum_j -\hat{u}_{\omega tj\iota}^\top \left(A_{\omega tj}X + e_{\omega tj}\right) - \hat{\mu}_{\omega tj\iota}\left(c_{\omega tj}^\top X + f_{\omega tj}\right), \qquad \iota = 1,2,..., \tag{35}$$

$$X \in \mathbb{X}, \tag{36}$$

in which, z is an ancillary variable; ι is the index of iterations.

The Generalized Benders Decomposition Algorithm solves the master problem (34)-(36) and the dual of every sub-problem (31)–(33) iteratively. In each iteration ι, an optimality cut (35) is added to the master problem to force its solution to converge to that of the original problem (26)–(28). The algorithm stops when a convergence criterion is met.

We prove that strong duality holds between the sub-problem (29)–(30) and its dual problem (31)–(33) in Appendix B. As a result, the cut (35) in each iteration is always effective, i.e., forcing the new master problem to obtain a better solution, before convergence.[7] Thus, the algorithm will converge to the global optimal solution after a finite number of iterations [33].

We utilize two techniques to accelerate the algorithm:

1) Relaxing the service ability constraint (8): Constraint (8) has no second stage decision variables but should be satisfied for every hour in every scenario (because of different traffic flows). However, it will be binding only in peak traffic hours in practice.[8] Therefore, we relax constraint (8) as follows:

$$y_i^{\text{cs}} \ge \sum_{q\in\mathcal{Q}_i}\sum_{k\in\mathcal{K}} T_k \lambda_{q,k,i,\hat{\omega t}_i}\gamma_{q,k,i} + \Phi^{-1}(\alpha)\sqrt{\sum_{q\in\mathcal{Q}_i}\sum_{k\in\mathcal{K}} T_k \lambda_{q,k,i,\hat{\omega t}_i}\gamma_{q,k,i}^2}, \quad \forall i \in \mathcal{I}, \tag{37}$$

where, $\hat{\omega t}_i$ is the index of the sub-problem that has the highest traffic flow at location i. We then add constraint (37) directly to the master problem and remove constraint (8) from every sub-problem. This approach leads to two benefits: 1) the scale of each sub-problem decreases significantly; 2) the modified sub-problem only solves an optimal power flow problem that allows load shedding which is strictly feasible given any X so that we need not consider feasibility cuts.[9]

2) Relaxing the integer constraints of the master problem: The master problem is computationally intensive for each iteration, since it contains a significant number of integer variables. We first relax its integer constraints and solve the problem (with higher efficiency) until convergence. Then, we add the integer constraints back to the master problem and conduct extra iterations until the new problem converges. Note that this approach will not affect the optimal solution because the feasible set of the original master problem is a subset of the relaxed master problem. Thus, the optimality cuts generated for the latter is also valid for the former [35].

The pseudo-code of the algorithm is shown in Table I. ε_1 and ε_2 are the relevant gaps at convergence of the original problem and its relaxed continuous form, respectively.

TABLE I
ACCELERATED GENERALIZED BENDERS DECOMPOSITION

01	**Initialization:** Set iteration number $\iota = 0$, lower bound $LB = -\infty$, upper bound $UB = +\infty$, relevant gap $Gap = +\infty$, $flag = 0$.
02	**While** termination criteria, i.e., $Gap \le \varepsilon_2$, not fulfilled, **do**
03	$\iota = \iota + 1$.
04	**Step 0** If $Gap \le \varepsilon_1$ and $flag = 0$, let $UB = +\infty$, $flag = 1$.
05	**Step 1** If $flag = 1$, solve master problem (34)–(36); otherwise, solve the relaxed continuous form of (34)–(36). Update the solution $\hat{X}$ and $\hat{z}$. Let $LB = c^T\hat{X} + \hat{z}$.
06	**Step 2** Solve each sub-problem's dual problem (31)–(33), and update each solution $\hat{u}_{\omega tj\iota}$ and $\hat{\mu}_{\omega tj\iota}$. Let $UB = \min\Big\{UB,\ c^T\hat{X} + \sum_{\omega\in\Omega}\sum_t\sum_j\Big(-\hat{u}_{\omega tj\iota}^\top\left(A_{\omega tj}\hat{X} + e_{\omega tj}\right) - \hat{\mu}_{\omega tj\iota}\left(c_{\omega tj}^\top\hat{X} + f_{\omega tj}\right)\Big)\Big\}$.
07	**Step 3** Add a new cut (35) for iteration ι to the master problem (34)–(36).
08	**Step 4** $Gap = 100\% \times (UB - LB)/UB$.
09	**End while**
10	**Output** $\hat{X}$ as the solution.

IV. CASE STUDIES AND CONCLUSIONS

A. Case Overview and Parameter Settings

We consider a 25-node highway transportation network (see Fig. 3) coupled with a 14-node 110 kV high voltage distribution network (see Fig. 4) to illustrate the proposed planning method.[10] The node coupling relationship between the distribution and transportation networks is also recorded in Fig. 4. We assume the power demand at each transportation node is supplied by its nearest distribution bus. The gravity spatial interaction model utilized in [37] was used to generate

[7] If the new cut did not force the master problem to obtain a new solution, then the LB and UB in Table I are equal so that the solution is optimal.

[8] If the constructed charging spots can satisfy peak-hour traffic flows' charging demands, they can also satisfy the demands during other periods.

[9] Note that, if constraint (8) is not relaxed and should be satisfied in every sub-problem, it may be violated given some myopic X. As a result, we should add extra iterations to generate feasibility cuts to the master problem.

[10] Note that we adopt the power system structure in China as the basis of this case study, where the 110 kV power networks are usually operated radially and categorized as high-voltage distribution systems [36].

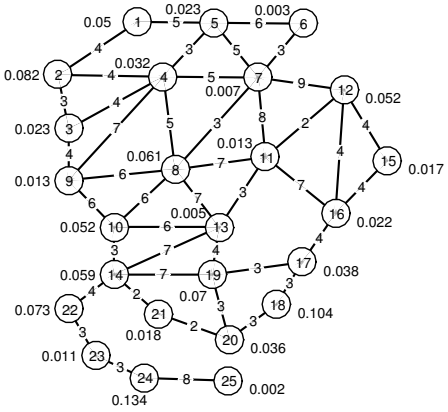

Fig. 3. A 25-node transportation network [38]. The number in each circle is the node index. The number on each arc represents the distance between the corresponding two nodes and the per-unit distance is 10 km. The decimal next to each node is its weight, which represents its traffic flow gravitation. To enhance network granularity, we add extra auxiliary nodes on the long road segments so that the longest distance between any two adjacent nodes is 20 km. As a result, the modified network has 93 nodes.

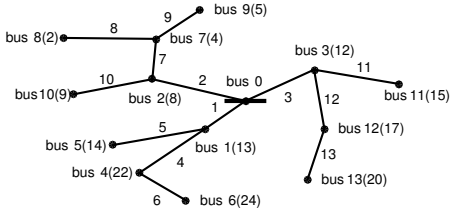

Fig. 4. A 110 kV distribution network used for the case study [37]. Bus 0 is connected to a 220 kV/110 kV transformer with 150 MVA capacity. The integer in each parenthesis denotes the corresponding index of transportation node in Fig. 3 where the distribution bus is located. The voltage constraints are $\underline{V_m} = 0.95$ and $\overline{V_m} = 1.05$, $\forall m$, in per unit values. The line current limits are conservatively set at 85% of their rated capacities.

the OD traveling demand based on node weights and arc distances. Due to limited space, the parameters of the distribution network and the details of the generated scenarios are omitted but can be found from [27].

There are 72 representative scenarios. This includes three types of weather conditions (rainy, cloudy, sunny) for typical weekdays and weekends, across twelve months. The hourly base load, traffic flow and PV power are generated based on PG&E load profiles [39], the National Household Travel Survey [40], and the National Solar Radiation Database [41].

We assume there are four types of PEVs on the road with equal market share, and their driving ranges per charge are 200, 300, 400 and 500 km, respectively. The rated charging power p^{sp} is 44 kW, and the average service time to charge the four types of PEVs with empty batteries are about 42, 63, 84, 105 minutes. We also assume $\overline{y_i^{\text{cs}}} = 200$ and $\alpha = 80\%$. The fixed cost for building one PEV charging station is $c_1 = \$163,000$ [42]. We consider that building a PEV charging station usually requires significant distribution grid upgrade costs. In this experiment, we assume that each charging station is connected to its nearest low/medium voltage substation which is further connected to the corresponding 110 kV bus. Building one charging station at transportation node i requires installing a low/medium voltage substation and a distribution line whose power capacities are both $\max_{\omega t} p_{i,\omega t}^{\text{ev}}$. The corresponding distribution line's length, l_i, is assumed to be 10% of the distance between the PEV charging station and its nearest 110 kV distribution bus. The per-unit costs for substations and distribution lines are 788 \$/kVA [43] and 120 \$/(kVA·km) [44], respectively. Hence, we let $c_2 = \$31,640 + (788 + 120 l_i) \max_{\omega t} p_{i,\omega t}^{\text{ev}}$ at each node i. The first term represents the costs for chargers, land use etc. [42]. The electricity purchase cost $c_{\text{e}}^{+} = 0.094$ \$/kWh and the selling price c_{e}^{-} is 30% lower. The per-unit penalty cost for unsatisfied charging demand $c_{\text{p}} = 10^3$ \$/kWh. The PV generation investment costs are $c_3 = 0$ \$/VA, $c_4 = 1,770$ \$/kVA [45]; $\sigma = \$10^{-4}$, $\zeta = \overline{8\%}(1+8\%)^{15}/((1+8\%)^{15}-1) = 0.1168$, $\overline{S^{\text{pv}}} = 90$ MVA, $\overline{y_m^{\text{pv}}} = \infty$ MVA, $\forall m$.[11]

TABLE II
THE PARAMETERS OF DIFFERENT CASES

Case	Max. total number/capacity of PV power plants	Reactive power control	Daily PEV traffic flow
1	0/0 MVA	–	20000
2	5/90 MVA	No	20000
3	5/90 MVA	Yes	20000
4	0/0 MVA	–	40000
5	5/90 MVA	No	40000
6	5/90 MVA	Yes	40000

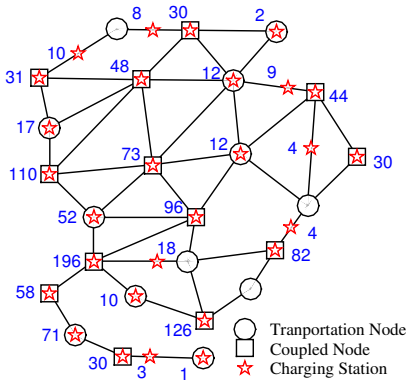

Fig. 5. Sites and sizes of PEV charging stations in Case 1. The number next to each station is its capacity, i.e., number of spots.

We design six cases, with different PEV traffic flows and maximum numbers of PV power plants with or without reactive power control to illustrate the proposed planning method. The parameters of different cases are illustrated in Table II.

We set algorithm parameters $\varepsilon_1 = 0.5\%$, $\varepsilon_2 = 2\%$ in Table I and use CPLEX [32] to solve the master problem and subproblems on a workstation with a 12 core Intel Xeon E5-1650 processor and 64 GB RAM. To accelerate the optimization speed, we relaxed y_i^{cs} to be continuous.

B. Planning Results and Analysis

The summary of the planning results for the six cases are given in Table III. The locations and capacities of PEV charging stations in Case 3 are given in Fig. 5 for demonstration. The PV generation and their capacities in different cases are illustrated in Fig. 6. The ratio of a line's current

[11]Note that there is usually enough land available in highway networks to build PV power plants. Therefore, we do not limit the $\overline{y_m^{\text{pv}}}$ here.

TABLE III
SUMMARY OF THE PLANNING RESULTS IN DIFFERENT CASES

Case	No. of stations	No. of spots	No. of PV power plants	PV capacity (MVA)	Investment costs (M$/year) PEV station	Investment costs (M$/year) PV power plants	Energy costs (M$/year)	Total costs (M$/year)	Unsatisfied PEV load (%)	Solution time (h)
1	33	1210	0	0.0	10.62	0.0	37.94	48.56	0.0	0.5
2	26	1187	4	71.52	9.75	14.79	22.47	47.01	0.0	16
3	28	1187	4	73.20	9.79	15.14	21.95	46.87	0.0	15
4	44	2279	0	0.0	23.97	0.0	48.39	72.37	1.85	1.8
5	31	2287	5	90	20.74	18.61	28.74	68.50	0.0	18
6	30	2285	4	90	21.03	18.61	28.53	68.17	0.0	18

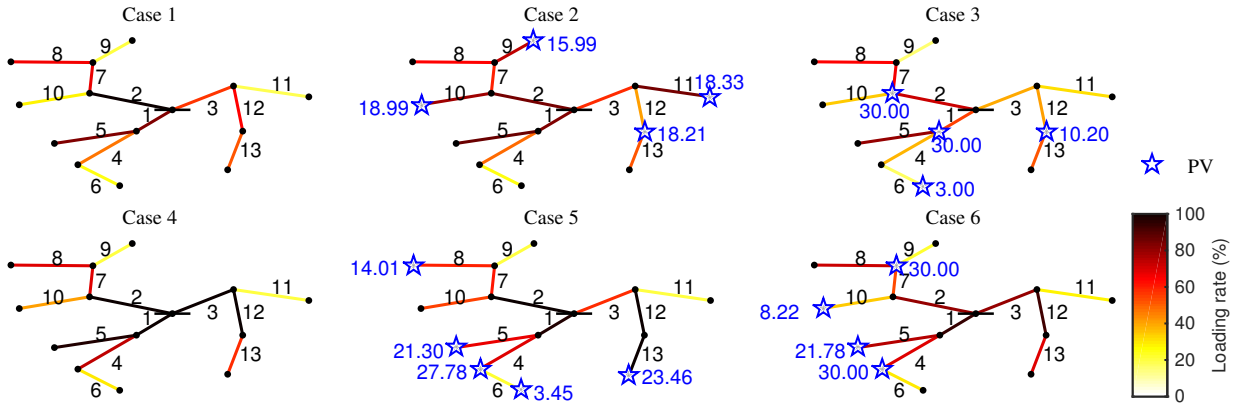

Fig. 6. Sites and sizes of PV power plants and loading rates of distribution lines. The number next to each PV power plant is its capacity, in MVA.

to its thermal capacity, i.e., $100\% \times \sqrt{l_{mn}}/\overline{I_{mn}}$, represents its loading rate. The maximum loading rate, i.e., $100\% \times \max_{\omega t}\left(\sqrt{l_{mn,\omega t}}/\overline{I_{mn}}\right)$, of each distribution line in the six cases are depicted by Colorbars in Fig. 6. The distributions of the line loading rates and nodal voltages in all the 24×72 hours are illustrated in Figs. 7–8, respectively.

1) Computational efficiency: When jointly planning PEV charging stations and PV power plants, the scale of the problem is larger; as a result, the solution time is also longer. When directly adopting the Branch-and-Bound Algorithm to solve the MISOCPs, the solver went out of memory. In contrast, the proposed Accelerated Generalized Benders Decomposition Algorithm can still solve the problems in less than 18 hours. Besides, the solution time is longer when the PEV population is larger. That is because larger PEV population leads to higher charging demands and more binding power flow constraints. As a result, the feasible set of the problem is smaller and the algorithm has to conduct more iterations to converge.

As mentioned earlier, we add extra auxiliary nodes on the long road segments to enhance network granularity so that the modified transportation network has 93 nodes. Though a network with 93 nodes may cover a large area for intercity scenarios, it is possible that some target transportation networks may be much larger than the studied case. In the proposed generalized Benders Decomposition Algorithm, the master problem is an MISOCP and the sub-problems are convex SOCPs. Though the sub-problems can be efficiently solved in parallel in polynomial time, the master problem's solution time (adopting the Branch-and-Bound algorithm) may grow exponentially with the scale of the transportation nodes. Hence, for large-scale transportation networks, the planing problem may still be intractable even with the proposed algorithm. Nevertheless, we can adopt different approaches to solve the problem at the cost of optimality, such as: 1) Decrease the granularity of the transportation network; 2) Increase the relevant gaps, ε_1 and ε_2, when the algorithm stops; 3) Divide the large-transportation network into several smaller sub-networks and solve the planning problem in each sub-network.

2) Direct financial benefit for saving total cost: The planning results show that by jointly building PEV charging stations and PV power plants, the total cost of the system is cut down: the total cost in Case 2 is reduced by 3.19% compared to Case 1 and the total cost in Case 5 is reduced by 5.35% compared to Case 4. Though the equivalent annual investment cost is increased, the installed PV power plants generate and sell electricity to the power grid, which significantly decreases the operational costs.

By utilizing distributed PV generation to supply power locally, the planner has larger flexibility to build PEV charging stations. Compared to Case 1 and Case 4, the overall investment costs on PEV charging stations and the corresponding power grid upgrades in both Case 2 and Case 5 are reduced. This phenomenon is especially prominent in heavy load scenarios. We can observe that in Case 4, much more charging stations are installed than in Case 5. Because some parts of the distribution system are congested, the planner has to build more charging stations elsewhere with higher costs to avoid the PEVs being charged at congested areas.

The total PV generation capacity and the direct financial

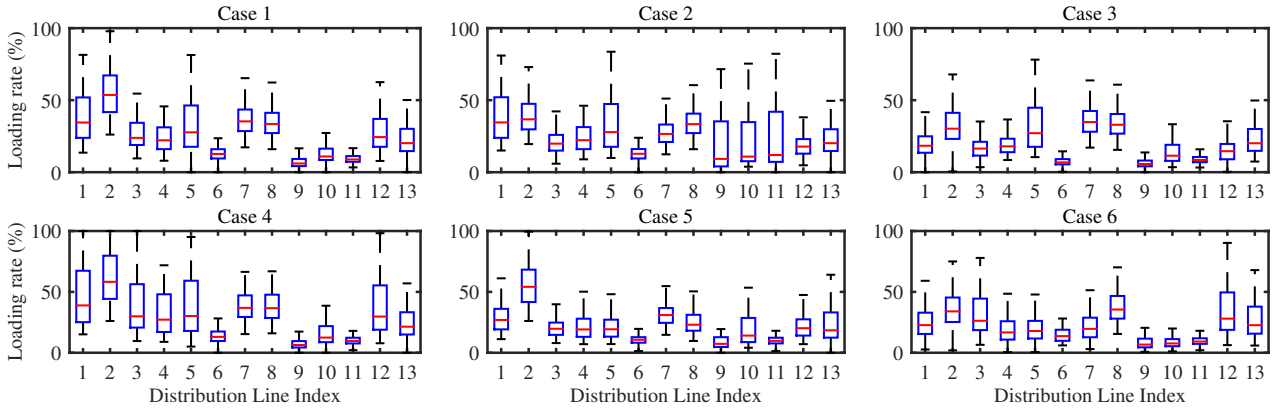

Fig. 7. Boxplot of distribution line thermal loading rates. Line 2 is typically the most congested.

benefit of integrating PEV charging stations with PV generation increase as the PEV population (or load) increases.

3) Indirect benefit by deferring power system investment: Figs. 6–7 show that investing distributed PV generation can significantly ease distribution line congestion, and therefore, defer power system investment. In Case 2, line 2 is the only one that is congested, which reflects the bottleneck of the system. In Case 4, several distribution lines' capacity constraints are binding, and as a result, 1.87% of the PEV charging demands cannot be satisfied. By contrast, in the cases with PV generation, no line is congested. Without building new PV power plants, the planner has to upgrade the congested distribution lines (line 2 would be the first choice), which would be much more expensive.

4) Benefit of utilizing reactive power control: By adopting reactive power control for PV generation, the system has larger operational flexibility. As a result, the total cost and the voltage deviations of the system are reduced. Though the monetary benefits seems to be insignificant (less than 1%'s total cost reduction), Fig. 8 shows that the system with reactive power control has much lower voltage deviations so that it can provide higher reliability electricity to customers. Note that, in both Case 2 and Case 4, we can observe significant voltage rises caused by inverse PV power flow. By contrast, in both Case 3 and Case 6, the voltage rises are mild. This advantage will also be much more pronounced at heavy load and high PV penetration scenarios when voltage drops and rises will significantly deteriorate the power quality.

C. Sensitivity Analysis

The planning results of the proposed model may be significantly affected by several important parameters such as the rated charging power of EV charging spots and the electricity price from the main grid. This section conducts sensitivity analyses on these parameters to validate their influence.

1) Rated charging power: In the previous experiments, we assumed the rated charging power of a charging spot, p^{sp}, to be 44 kW. We adjust this value to its 50%, 75%, 125% and 150%, then adopt the proposed method to reoptimize the PEV charging stations and PV power plants. In these experiments, we assume that the variable cost to buy a charging spot is proportional to its rated charging power. The total invested numbers of charging spots, capacities of PV power plants are illustrated in Fig. 9. As expected, when the rated charging power increases, the total number of charging spots decreases. This is also indicated in the quality of service constraint (8): with higher rated charging power, the mean charging time of PEVs, $T_k, \forall k \in \mathcal{K}$, decreases so that the same volume of charging requests can be satisfied by fewer charging spots. However, we can observe that the invested capacity of PV power plants is insignificantly affected by rated PEV charging power. That is because changing rated charging power will not affect the total energy consumption of the PEVs. Besides, when a single PEV's charging power increases or decreases, the number of PEVs charging at the same time will inversely decrease or increase. As a result, the hourly average charging power profiles of the charging stations are not affected significantly.

2) Electricity price from main grid: The total invested numbers of charging spots and capacities of PV power plants to install with different electricity prices from the main grid are illustrated in Fig. 10. Because the penalty for unsatisfied PEV charging demands is high, the investment in PEV charging stations is not sensitive to the electricity price. In contrast, the investment in PV power plants are remarkably affected by the electricity price. When the electricity price rises, it is more expensive to buy electricity from the main grid. As a result, the system tends to install more PV power plants to boost local power supply.

V. Conclusion

This paper develops a two-stage stochastic SOCP for jointly planning PEV fast-charging stations and distributed PV power plants on coupled transportation and power networks. This model incorporates comprehensive models of 1) transportation networks with explicit PEV driving range constraints; 2) PEV charging stations with probabilistic quality of service constraints; 3) PV power generation with reactive power

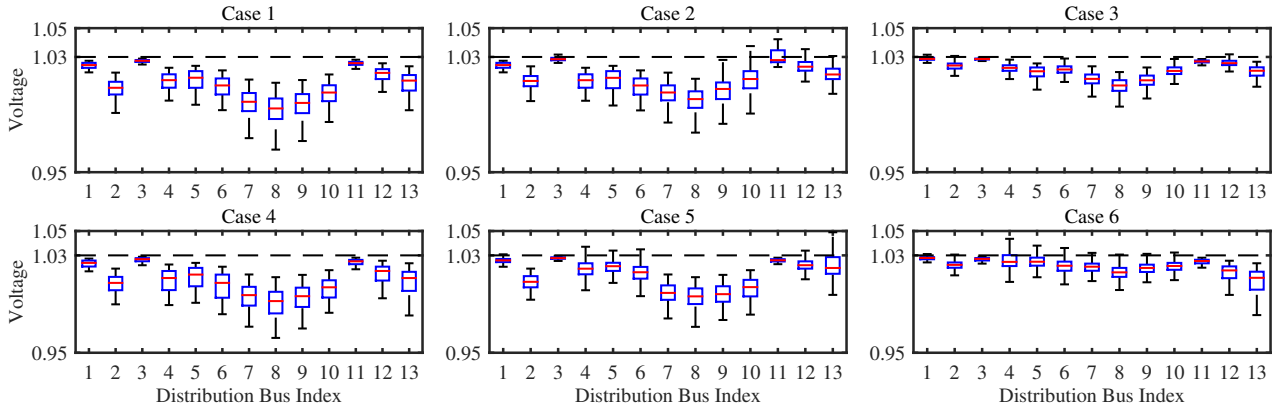

Fig. 8. Boxplot of voltages. The reference voltage is 1.03 at root bus 0.

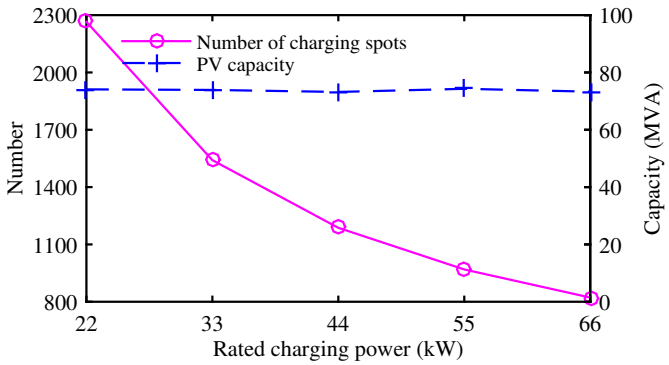

Fig. 9. Sensitivity analysis on rated charging power.

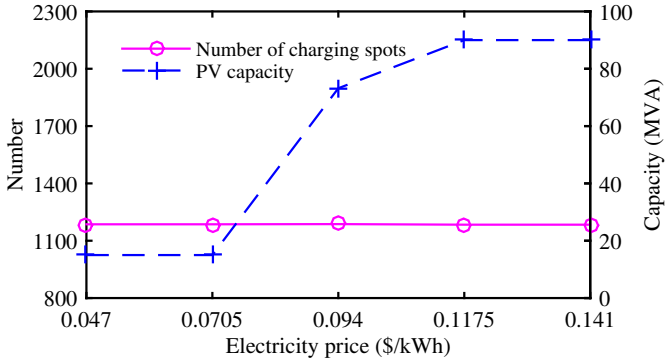

Fig. 10. Sensitivity analysis on electricity price.

control; and 4) alternating current distribution power flow. The formulation results in a MISOCP. To address the uncertainty of future scenarios, a significant number of future typical load, traffic flow and PV generation curves are adopted. This makes the problem large scale. We then design a Generalized Benders Decomposition Algorithm to efficiently solve the program by decoupling it into an MISOCP master problem and a set of convex SOCP sub-problems.

We conduct numerical experiments to illustrate the effectiveness of the proposed method and quantify the benefits of the joint planning model. Simulation results show that jointly planning PEV charging stations and PV power plants can significantly reduce total investment and operation costs for the system. Compared with scenarios when only PEV charging stations are constructed, jointly investing in PEV charging stations and PV power plants can reduce total costs by 3.19% to 5.35%. The direct financial benefit of integrating PEV charging stations with PV generation increases with the PEV population. Jointly planing distributed PEV charging stations and PV power plants can also help alleviate power congestion caused by large-scale PEV integration. This will thereafter defer the demand for expensive investment in power system upgrades. The aforementioned benefits become more prominent when utilizing PV generation with reactive power control which can help reduce voltage deviations and enhance power supply quality. This advantage will also be much more pronounced at heavy load and high PV penetration scenarios when voltage drops and rises will significantly deteriorate the power quality. Sensitivity analyses show that the required number of PEV charging spots in the system decrease when the rated PEV charging power rises; the capacity of PV power plants is very sensitive to the electricity price from the main grid.

Though the proposed Generalized Benders Decomposition Algorithm can help accelerate the optimization for cases with a large number of uncertain scenarios, it still has non-negligible limitation on handling large transportation networks that require large-scale binary variables for charging station investment decisions. Efficient algorithms for planning in large-scale transportation networks will be our future focus. Energy storage systems can help balance power supply and demand in the distribution systems. This will further promote synergies between PV generation, PEV charging demands, and other distributed resources. Joint planning PEV charging station and PV power plants with energy storage systems is also an interesting future research topic.

APPENDIX A
THE DUAL PROBLEM

A. The Full Formulation of the Sub-problem

Given a fixed first stage solution $\hat{X}$, the sub-problem ωt is a convex SOCP, as follows (the index ωt in the variables is omitted for brevity):

$$\min_{Y} \left\{ \left(c_{\mathrm{e}}^{+} p_0^{+} - c_{\mathrm{e}}^{-} p_0^{-}\right) \Delta t + \sum_{m\in\mathcal{M}_+} c_{\mathrm{p}} p_m^{\mathrm{loss}} \Delta t + \sum_{m\in\mathcal{M}_+} \sigma v_m^{\mathrm{d}} \right\}, \tag{38}$$

$$\text{s.t.: } \forall i \in \mathcal{I}, \forall m \in \mathcal{M}_+, \forall (m,n) \in \mathcal{B}:$$

$$\sqrt{|p_m^{\mathrm{pv}}|^2 + |q_m^{\mathrm{pv}}|^2} \le y_m^{\mathrm{pv}}, \tag{39}$$

$$0 \le p_m^{\mathrm{pv}} \le \overline{p_m^{\mathrm{pv}}}, \tag{40}$$

$$s_m^{\mathrm{pv}} = p_m^{\mathrm{pv}} + j q_m^{\mathrm{pv}}, \tag{41}$$

$$S_{mn} = s_m + \sum_{h\in\mathcal{M}_m} (S_{hm} - z_{hm} l_{hm}), \tag{42}$$

$$0 = s_0 + \sum_{h\in\mathcal{M}_0} (S_{h0} - z_{h0} l_{h0}), \tag{43}$$

$$v_m - v_n = 2\mathrm{Re}(z_{mn}^{*} S_{mn}) - |z_{mn}|^2 l_{mn}, \tag{44}$$

$$|S_{mn}|^2 \le l_{mn} v_m, \tag{45}$$

$$s_m = s_m^{\mathrm{pv}} - s_m^{\mathrm{ev}} - s_m^{\mathrm{b}} = p_m + j q_m, \tag{46}$$

$$p_0 = p_0^{+} - p_0^{-}, \tag{47}$$

$$s_m^{\mathrm{ev}} = p_m^{\mathrm{ev}}, \tag{48}$$

$$p_m^{\mathrm{ev}} + p_m^{\mathrm{loss}} = \sum_{i\in\mathcal{I}_m} p_i^{\mathrm{ev}}, \tag{49}$$

$$p_i^{\mathrm{ev}} = p^{\mathrm{sp}} \sum_{q\in\mathcal{Q}_i} \sum_{k\in\mathcal{K}} T_k \lambda_{q,k} \gamma_{q,k,i}, \tag{50}$$

$$0 \le l_{mn} \le |\overline{I_{mn}}|^2, \tag{51}$$

$$|\underline{V_m}|^2 \le v_m \le |\overline{V_m}|^2. \tag{52}$$

$$v_m^{\mathrm{d}} \ge v_m - v_0 \tag{53}$$

$$v_m^{\mathrm{d}} \ge -v_m + v_0 \tag{54}$$

$$p_m^{\mathrm{loss}} \ge 0, \tag{55}$$

in which, v_m^{d} is the nodal voltage deviation compared to the reference v_0 (at root bus 0). The objective (38) is linear; constraints (39) and (45) are second order cones; the other constraints are all affine. The decision variables $Y = \{l_{mn}, p_i^{\mathrm{ev}}, p_m^{\mathrm{loss}}, s_0, s_m^{\mathrm{pv}}, s_m^{\mathrm{ev}}, S_{mn}, v_m, v_m^{\mathrm{d}}, \forall i \in \mathcal{I}, \forall m \in \mathcal{M}_+, \forall (m,n) \in \mathcal{B}\}$ are all continuous.

We let $\mathcal{D}$ denote the domain of the sub-problem (38)–(55), i.e., the intersection of the domains of the objective and the constraint functions of (38)–(55). It's obvious that $\mathcal{D} = \mathbf{R}^d =$ relint $\mathcal{D}$ (d is the dimension of Y).

B. The Sub-problem's Dual Problem

For simplicity, we reformulate the sub-problem (38)–(55) in its standard form:

$$p^{*} = \min_{Y} \ d^{\top} Y \tag{56}$$

$$\text{s.t.: } \|B_j Y + A_j \hat{X} + e_j\|_2 \le d_j^{\top} Y + c_j^{\top} \hat{X} + f_j, \quad \forall j, \tag{57}$$

in which p^{*} is the primal objective.

We follow the procedure in [34] to obtain its dual problem. First, we have

$$p^{*} = \inf_{Y} \sup_{\mu\ge 0} \ d^{\top} Y + \sum_j \mu_j \left(\|B_j Y + A_j \hat{X} + e_j\|_2 - \left(d_j^{\top} Y + c_j^{\top} \hat{X} + f_j \right) \right) \tag{58}$$

$$= \inf_{Y} \sup_{\|u_j\|_2 \le \mu_j, \forall j} \ d^{\top} Y + \sum_j \left(-u_j^{\top} \left(B_j Y + A_j \hat{X} + e_j \right) - \mu_j \left(d_j^{\top} Y + c_j^{\top} \hat{X} + f_j \right) \right), \tag{59}$$

where we have used the dual representation of the Euclidean norm. μ_j is the dual variable vector of each second order cone and u_j is the dual variable vector of each Euclidean norm.

Then, adopting the max-min inequality [34], we have

$$d^{*} = \sup_{\|u_j\|_2 \le \mu_j, \forall j} \inf_{Y} \ d^{\top} Y + \sum_j \left(-u_j^{\top} \left(B_j Y + A_j \hat{X} + e_j \right) - \mu_j \left(d_j^{\top} Y + c_j^{\top} \hat{X} + f_j \right) \right), \tag{60}$$

which makes $d^{*} \le q^{*}$.

Solving (60) for variable Y, we obtain the dual problem:

$$d^{*} = \sup_{\mu_j, u_j, \forall j} \left\{ \sum_j -u_j^{\top} \left(A_j \hat{X} + e_j \right) - \mu_j \left(c_j^{\top} \hat{X} + f_j \right) \right\} \tag{61}$$

$$\text{s.t.: } \sum_j \left(B_j^{\top} u_j + \mu_j d_j \right) = d, \tag{62}$$

$$\|u_j\|_2 \le \mu_j, \qquad \forall j, \tag{63}$$

which is still a convex SOCP.

APPENDIX B
PROOF OF STRONG DUALITY

A. The Slater's Condition

The Slater's Condition provides a sufficient condition for strong duality. We give a brief introduction for it in this part.

For a convex optimization problem:

$$p^{*} = \min_{x} \ f_0(x) \tag{64}$$

$$\text{s.t.: } f_i(x) \le 0, \qquad i = 1, ..., m, \tag{65}$$

$$h_i(x) = 0, \qquad i = 1, ..., q, \tag{66}$$

we still let $\mathcal{D}$ denote the domain of the problem. Then, we have the following proposition:

Proposition 1 (Slater's conditions for convex programs) *Let $f_i, i = 0, ..., m$, be convex functions, and let $h_i, i = 0, ..., q$, be affine functions. Suppose further that the first $k \le m$ of the f_i functions, $i = 1, ..., k$, are affine (or let $k = 0$, if none of the $f_i, i = 0, ..., m$, is affine). If there exists a point $x \in$ relint $\mathcal{D}$ such that*

$$f_i(x) \le 0, \qquad i = 1, ..., k, \tag{67}$$

$$f_i(x) < 0, \qquad i = k+1, ..., m, \tag{68}$$

$$h_i(x) = 0, \qquad i = 1, ..., q, \tag{69}$$

then strong duality holds between the primal problem (64)–(66) and its dual problem. Moreover, if the primal problem is

bounded, i.e., $p^* > -\infty$, then the dual optimal value equals to the primal optimal value. [34]

In the following section, we will use the above proposition to prove strong duality of the sub-problem (56)–(57) and its dual problem (61)–(63). We say an inequality constraint to be "strictly satisfied" to refer to that it is "satisfied with strict inequality" as (68).

B. Proof of Strong Duality

We assume that the system can be operated without PV generation and PEV charging power, and the constraints of nodal voltages of the distribution system is not binding. Note that this is a very mild assumption, because the distribution system is usually operated with the voltage deviations being well controlled. Otherwise, the power quality is poor and extra voltage control devices should be installed for the system.

We first let $s_m^{\text{pv}} = 0$ and $s_m^{\text{ev}} = 0$, $\forall m \in \mathcal{M}_+$. With constraints (49)–(50), we can directly calculate variables $p_i^{\text{ev}} = 0$ and $p_m^{\text{loss}} = p^{\text{sp}} \sum_{i\in\mathcal{I}_m} \sum_{q\in\mathcal{Q}_i} \sum_{k\in\mathcal{K}} T_k \lambda_{q,k} \gamma_{q,k,i}$, $\forall m \in \mathcal{M}_+$. As a result, the sub-problem (38)–(55) is reduced to a simple optimal AC power flow problem. Based on the above assumption, there is a feasible solution $Y^* = \{l_{mn}, p_i^{\text{ev}}, p_m^{\text{loss}}, s_0, s_m^{\text{pv}}, s_m^{\text{ev}}, S_{mn}, v_m, v_m^{\text{d}}, \forall i \in \mathcal{I}, \forall m \in \mathcal{M}_+, \forall (m,n) \in \mathcal{B}\} \in$ relint $\mathcal{D}$ subjects to:

$$|\underline{V_m}|^2 < v_m < |\overline{V_m}|^2, \qquad \forall m \in \mathcal{M}_+. \tag{70}$$

Furthermore, $\exists \Delta v > 0$, subjects to:

$$|\underline{V_m}|^2 < v_m + \Delta v \le |\overline{V_m}|^2, \qquad \forall m \in \mathcal{M}_+. \tag{71}$$

When $s_m^{\text{pv}} = 0$, $\forall m \in \mathcal{M}_+$, the active and reactive power injection at each node (except the root node 0) are both negative. Therefore, the distribution system have nonzero unidirectional power flows so that we also have:

$$l_{mn} > 0, \qquad \forall (m,n) \in \mathcal{B}. \tag{72}$$

There are only two non-affine constraints in each sub-problem, i.e., PV generation constraint (39) and AC power flow constraint (45). We discuss how we can construct a feasible solution based on Y^* which strictly satisfies (39) and (45).

1) PV generation: In the first non-affine constraint (39), the nameplate apparent power, i.e., $y_m^{\text{pv}}, \forall m \in \mathcal{M}_+$, are nonnegative and given by the master problem. $\forall m \in \mathcal{M}_+$: a)

1) If $y_m^{\text{pv}} = 0$, there is no PV generation at bus m so that constraints (39)–(41) can be omitted;
2) Otherwise, $y_m^{\text{pv}} > 0$, for $s_m^{\text{pv}} = 0$ in Y^*, it satisfies

$$\sqrt{|p_m^{\text{pv}}|^2 + |q_m^{\text{pv}}|^2} = 0 < y_m^{\text{pv}}, \quad \forall m \in \mathcal{M}_+. \tag{73}$$

Therefore, $\forall m \in \mathcal{M}_+$, if $y_m^{\text{pv}} = 0$, constraint (39) can be omitted; otherwise, it is strictly satisfied for $s_m^{\text{pv}} = 0$.

2) AC power flow: We slightly increase $v_m, \forall m \in \mathcal{M}_+$, in Y^* by the Δv in constraint (71) and adjust the corresponding nodal voltage deviations, i.e., $v_m^{\text{d}}, \forall m \in \mathcal{M}_+$, to construct another solution $Y^{**} = \{l_{mn}, p_i^{\text{ev}}, p_m^{\text{loss}}, s_0, s_m^{\text{pv}}, s_m^{\text{ev}}, S_{mn}, \hat{v}_m = v_m + \Delta v, \hat{v}_m^{\text{d}} = \max\{v_m^{\text{d}}, v_m^{\text{d}} + \Delta v\}, \forall i \in \mathcal{I}, \forall m \in \mathcal{M}_+, \forall (m,n) \in \mathcal{B}\} \in$ relint $\mathcal{D}$. The other variables are equal to those in Y^*. Then, we have

$$\forall m \in \mathcal{M}_+, \forall (m,n) \in \mathcal{B}:$$
$$\hat{v}_m - \hat{v}_n = v_m - v_n, \tag{74}$$
$$|\underline{V_m}|^2 \le \hat{v}_m = v_m + \Delta v \le |\overline{V_m}|^2, \tag{75}$$
$$|S_{mn}|^2 \le l_{mn} v_m < l_{mn}(v_m + \Delta v) = l_{mn} \hat{v}_m, \tag{76}$$

As a result, the new solution Y^{**} is still feasible and strictly satisfies the non-affine constraint (45), i.e., (76). Besides, from Appendix B-B1, we also know that Y^{**} strictly satisfies constraint (39), when $y_m^{\text{pv}} > 0$.

To conclude, $Y^{**} \in$ relint $\mathcal{D}$ is a feasible solution for the sub-problem (38)–(55), i.e., problem (56)–(57), and it strictly satisfies all the non-affine constraints. Based on Proposition 1, we can conclude that strong duality holds between the sub-problem (56)–(57) and its dual problem (61)–(63).

Moreover, because the total PV generation is constrained, the selling power of the system, i.e., p_0^-, is limited and the second term in (38) is bounded below. The other terms in (38) are all nonnegative. Thus, we can conclude that the sub-problem's objective (38) is bounded below. As a result, there exist a primal solution Y^{**} and a dual solution $\{\mu^*, u^*\}$ that let the primal optimal objective p^* equal to the dual optimal objective q^*.

REFERENCES

[1] A. Elgowainy, A. Burnham, M. Wang, J. Molburg, and A. Rousseau, "Well-to-wheels energy use and greenhouse gas emissions of plug-in hybrid electric vehicles," *SAE Int. J. Fuels Lubr.*, vol. 2, no. 2009-01-1309, pp. 627–644, 2009.

[2] Chinadaily, "China to build 12,000 nev chargers by 2020." [Online]. Available: http://www.chinadaily.com.cn/business/motoring/2015-10/13/content_22170160.htm, accessed Sep 30, 2016.

[3] M. Takagi, Y. Iwafune, K. Yamaji, H. Yamamoto, K. Okano, R. Hiwatari, and T. Ikeya, "Economic Value of PV Energy Storage Using Batteries of Battery-Switch Stations," *IEEE Trans. Sustain. Energy*, vol. 4, no. 1, pp. 164–173, 2013.

[4] N. MacHiels, N. Leemput, F. Geth, J. Van Roy, J. Buscher, and J. Driesen, "Design criteria for electric vehicle fast charge infrastructure based on flemish mobility behavior," *IEEE Trans. Smart Grid*, vol. 5, no. 1, pp. 320–327, 2014.

[5] M. Brenna, a. Dolara, F. Foiadelli, S. Leva, and M. Longo, "Urban Scale Photovoltaic Charging Stations for Electric Vehicles," *IEEE Trans. Sustain. Energy*, vol. 5, no. 4, pp. 1234–1241, 2014.

[6] Y.-T. Liao and C.-N. Lu, "Dispatch of EV Charging Station Energy Resources for Sustainable Mobility," *IEEE Trans. Transport. Electric.*, vol. 1, no. 1, pp. 86–93, 2015.

[7] D. Wu, H. Zeng, C. Lu, and B. Boulet, "Two-stage energy management for office buildings with workplace ev charging and renewable energy," *IEEE Trans. Transport. Electrific.*, vol. 3, no. 1, pp. 225–237, 2017.

[8] M. J. E. Alam, K. M. Muttaqi, and D. Sutanto, "Effective Utilization of Available PEV Battery Capacity for Mitigation of Solar PV Impact and Grid Support with Integrated V2G Functionality," *IEEE Trans. Smart Grid*, vol. 7, no. 3, pp. 1562–1571, 2016.

[9] N. Liu, Z. Chen, J. Liu, X. Tang, X. Xiao, and J. Zhang, "Multi-objective optimization for component capacity of the photovoltaic-based battery switch stations: Towards benefits of economy and environment," *Energy*, vol. 64, pp. 779–792, 2014.

[10] G. Chandra Mouli, P. Bauer, and M. Zeman, "System design for a solar powered electric vehicle charging station for workplaces," *Appl. Energy*, vol. 168, pp. 434–443, 2016.

[11] D. Quoc, Z. Yang, and H. Trinh, "Determining the size of PHEV charging stations powered by commercial grid-integrated PV systems considering reactive power support," *Appl. Energy*, vol. 183, pp. 160–169, 2016.

[12] J. Ugirumurera and Z. J. Haas, "Optimal capacity sizing for completely green charging systems for electric vehicles," *IEEE Trans. Transport. Electrific.*, vol. 3, no. 3, pp. 565–577, 2017.

[13] B. Zhang, Q. Yan, and M. Kezunovic, "Placement of ev charging stations integrated with pv generation and battery storage," in *2017 Twelfth International Conference on Ecological Vehicles and Renewable Energies (EVER)*, pp. 1–7, April 2017.

[14] M. F. Shaaban and E. F. El-Saadany, "Accommodating high penetrations of pevs and renewable DG considering uncertainties in distribution systems," *IEEE Trans. Power Syst.*, vol. 29, no. 1, pp. 259–270, 2014.

[15] M. H. Moradi, M. Abedini, S. R. Tousi, and S. M. Hosseinian, "Optimal siting and sizing of renewable energy sources and charging stations simultaneously based on Differential Evolution algorithm," *Int. J. Elec. Power.*, vol. 73, pp. 1015–1024, 2015.

[16] M. H. Amini, M. P. Moghaddam, and O. Karabasoglu, "Simultaneous Allocation of Electric Vehicles ' Parking Lots and Distributed Renewable Resources in Power Distribution Network," *Sustain. Cities Soc.*, vol. 28, pp. 332–342, 2017.

[17] K. Kasturi and M. R. Nayak, "Optimal planning of charging station for evs with pv-bes unit in distribution system using woa," in *Man and Machine Interfacing (MAMI), 2017 2nd International Conference on*, pp. 1–6, IEEE, 2017.

[18] O. Erdinç, A. Taşcıkaraoğlu, N. G. Paterakis, İ. Dursun, M. C. Sinim, and J. P. Catalão, "Comprehensive optimization model for sizing and siting of dg units, ev charging stations and energy storage systems," *IEEE Transactions on Smart Grid*, 2017.

[19] P. M. de Quevedo, G. Muñoz-Delgado, and J. Contreras, "Impact of electric vehicles on the expansion planning of distribution systems considering renewable energy, storage and charging stations," *IEEE Transactions on Smart Grid*, 2017.

[20] H. Dashti, A. J. Conejo, R. Jiang, and J. Wang, "Weekly two-stage robust generation scheduling for hydrothermal power systems," *IEEE Trans. Power Syst.*, vol. 31, no. 6, pp. 4554–4564, 2016.

[21] C. Shao, X. Wang, X. Wang, C. Du, and B. Wang, "Hierarchical charge control of large populations of evs," *IEEE Trans. Smart Grid*, vol. 7, no. 2, pp. 1147–1155, 2016.

[22] X. Tan, G. Qu, B. Sun, N. Li, and D. H. Tsang, "Optimal scheduling of battery charging station serving electric vehicles based on battery swapping," *IEEE Trans. Smart Grid*, 2017.

[23] Y. Wen, C. Guo, H. Pandzic, and D. S. Kirschen, "Enhanced security-constrained unit commitment with emerging utility-scale energy storage," *IEEE Trans. Power Syst.*, vol. 31, no. 1, pp. 652–662, 2016.

[24] C. Dai, L. Wu, and H. Wu, "A multi-band uncertainty set based robust scuc with spatial and temporal budget constraints," *IEEE Trans. Power Syst.*, vol. 31, no. 6, pp. 4988–5000, 2016.

[25] A. Bagheri, J. Wang, and C. Zhao, "Data-driven stochastic transmission expansion planning," *IEEE Trans. Power Syst.*, vol. 32, no. 5, pp. 3461–3470, 2017.

[26] H.-Y. Mak, Y. Rong, and Z.-J. M. Shen, "Infrastructure planning for electric vehicles with battery swapping," *Manag. Sci.*, vol. 59, no. 7, pp. 1557–1575, 2013.

[27] H. Zhang, S. J. Moura, Z. Hu, W. Qi, and Y. Song, "A Second-Order Cone Programming Model for Planning PEV Fast-Charging Stations," *IEEE Trans. Power Syst.*, vol. 33, pp. 2763–2777, May 2018.

[28] B. K. Turitsyn, M. Ieee, S. Backhaus, and M. Chertkov, "Options for control of reactive power by distributed photvoltaic generators," *Proc. IEEE.*, vol. 99, no. 6, pp. 1063–1073, 2011.

[29] E. Dallranese, S. V. Dhople, and G. B. Giannakis, "Optimal Dispatch of Photovoltaic Inverters in Residential Distribution Systems," *IEEE Trans. Sustain. Energy*, vol. 5, no. 2, pp. 487–497, 2014.

[30] M. E. Baran and F. F. Wu, "Optimal capacitor placement on radial distribution systems," *IEEE Trans. Power Del.*, vol. 4, no. 1, pp. 725–734, 1989.

[31] M. Farivar and S. H. Low, "Branch flow model: Relaxations and convexification–part I," *IEEE Trans. Power Syst.*, vol. 28, no. 3, pp. 2554–2564, 2013.

[32] IBM, "Ibm ilog cplex optimization studio 12.5." [Online]. Available: http://www-01.ibm.com/support/knowledgecenter/SSSA5P_12.5.1/maps/ic-homepage.html, accessed Feb 15, 2015.

[33] D. Mcdanielt and M. Devine, "A Modified Benders' Partitioning Algorithm for Mixed Integer Programming," *Manag. Sci.*, vol. 24, no. 3, pp. 312–319, 1977.

[34] G. Calafiore and L. El Ghaoui, *Optimization Models*. Control systems and optimization series, Cambridge University Press, October 2014.

[35] A. M. Costa, B. Gendron, and G. Laporte, "Accelerating Benders Decomposition With Heuristic Master Problem Solutions," *Pesquisa Operacional (2012)*, vol. 32, no. 1, pp. 3–19, 2012.

[36] J. Zhong, C. Wang, and Y. Wang, "Chinese growing pains," *IEEE power & energy magazine*, vol. 5, no. 4, pp. 33–40, 2007.

[37] H. Zhang, S. J. Moura, Z. Hu, and Y. Song, "PEV Fast-Charging Station Siting and Sizing on Coupled Transportation and Power Networks," *IEEE Trans. Smart Grid*, to be published, doi: 10.1109/TSG.2016.2614939.

[38] D. Simchi-Levi and O. Berman, "A heuristic algorithm for the traveling salesman location problem on networks," *Operations research*, vol. 36, no. 3, pp. 478–484, 1988.

[39] PG&E, "2000 static load profiles." [Online]. Available: https://www.pge.com/nots/rates/2000_static.shtml, accessed Sep 30, 2016.

[40] A. Santos, N. McGuckin, H. Y. Nakamoto, D. Gray, and S. Liss, "Summary of travel trends: 2009 national household travel survey," tech. rep., 2011.

[41] NREL, "National solar radiation data base 1991-2010 update." [Online]. Available: http://rredc.nrel.gov/solar/old_data/nsrdb/1991-2010/, accessed Sep 30, 2016.

[42] H. Zhang, Z. Hu, Z. Xu, and Y. Song, "An Integrated Planning Framework for Different Types of PEV Charging Facilities in Urban Area," *IEEE Trans. Smart Grid*, vol. 7, no. 5, pp. 2273–2284, 2016.

[43] W. Yao, J. Zhao, F. Wen, Z. Dong, Y. Xue, Y. Xu, and K. Meng, "A multi-objective collaborative planning strategy for integrated power distribution and electric vehicle charging systems," *IEEE Trans. Power Syst.*, vol. 29, no. 4, pp. 1811–1821, 2014.

[44] W. Yao, C. Y. Chung, F. Wen, M. Qin, and Y. Xue, "Scenario-based comprehensive expansion planning for distribution systems considering integration of plug-in electric vehicles," *IEEE Trans. Power Syst.*, vol. 31, no. 1, pp. 317–328, 2016.

[45] D. Chung, C. Davidson, R. Fu, K. Ardani, and R. Margolis, "U.S. Photovoltaic Prices and Cost Breakdowns : Q1 2015 Benchmarks for Residential , Commercial , and Utility-Scale Systems," *National Renewable Energy Laboratory*, no. September, 2015.

Hongcai Zhang (S'14–M'18) received the B.S. and Ph.D. degree in electrical engineering from Tsinghua University, Beijing, China, in 2013 and 2018, respectively. In 2016–2017, he worked as a visiting student researcher in the Energy, Controls, and Applications Lab at University of California, Berkeley, where he is currently working as a postdoctoral scholar.

His current research interests include optimal planning and operation of power and transportation systems, grid integration of distributed energy resources.

Scott J. Moura (S'09–M'13) received the B.S. degree from the University of California, Berkeley, CA, USA, and the M.S. and Ph.D. degrees from the University of Michigan, Ann Arbor, MI, USA, in 2006, 2008, and 2011, respectively, all in mechanical engineering.

He is currently an Assistant Professor and Director of the Energy, Controls, and Applications Laboratory (eCAL) in Civil & Environmental Engineering at the University of California, Berkeley. He is also an Assistant Professor with the Smart Grid and Renewable Energy Laboratory, Tsinghua-Berkeley Shenzhen Institute. In 2011-2013, he was a postdoctoral fellow at the Cymer Center for Control Systems and Dynamics at the University of California, San Diego. In 2013 he was a visiting researcher in the Centre Automatique et Systèms at MINES ParisTech in Paris, France. His current research interests include optimal and adaptive control, partial differential equation control, batteries, electric vehicles, and energy storage.

Dr. Moura is a recipient of the National Science Foundation Graduate Research Fellowship, UC Presidential Postdoctoral Fellowship, O. Hugo Shuck Best Paper Award, ACC Best Student Paper Award (as advisor), ACC and ASME Dynamic Systems and Control Conference Best Student Paper Finalist (as student), Hellman Fellows Fund, University of Michigan Distinguished ProQuest Dissertation Honorable Mention, University of Michigan Rackham Merit Fellowship, College of Engineering Distinguished Leadership Award.

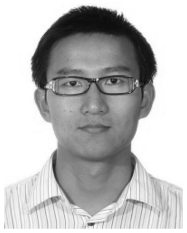

Zechun Hu (M'09–SM'17) received the B.S. and Ph.D. degrees in electrical engineering from Xi'an Jiao Tong University, Xi'an, China, in 2000 and 2006, respectively.

He worked in Shanghai Jiao Tong University after graduation and also worked in University of Bath as a research officer from 2009 to 2010. He joined the Department of Electrical Engineering at Tsinghua University in 2010 where he is now an associate professor. He serves as an associate editor of IEEE Transactions on Transportation Electrification. His major research interests include optimal planning and operation of power systems, electric vehicles and energy storage systems.

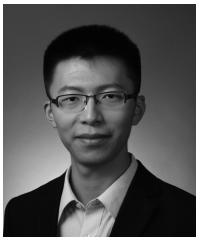

Wei Qi received the B.S. degree in control science and engineering from Zhejiang University, Hangzhou, China, M.S. degree in chemical engineering from University of California, Los Angeles, CA, USA, and the Ph.D. degree in the Department of Industrial Engineering and Operations Research, University of California, Berkeley, CA, USA, in 2010, 2011, 2015, respectively.

He is currently an assistant professor in Operations Management at the Desautels Faculty of Management, McGill University. In 2016–2017, he was a postdoc fellow in the China Energy Group, Energy Analysis and Environmental Impacts Division at the Lawrence Berkeley National Laboratory.

His research focuses on energy and transportation systems optimization, emerging techno-economic models, sustainable operations, supply chain design and management, and data analytics.

Yonghua Song (F'08) received the B.E. and Ph.D. degrees from the Chengdu University of Science and Technology, Chengdu, China, and the China Electric Power Research Institute, Beijing, China, in 1984 and 1989, respectively, all in electrical engineering.

From 1989 to 1991, he was a Post-Doctoral Fellow at Tsinghua University, Beijing. He then held various positions at Bristol University, Bristol, U.K.; Bath University, Bath, U.K.; and John Moores University, Liverpool, U.K., from 1991 to 1996. In 1997, he was a Professor of Power Systems at Brunel University, where he was a Pro-Vice Chancellor for Graduate Studies since 2004. In 2007, he took up a Pro-Vice Chancellorship and Professorship of Electrical Engineering at the University of Liverpool, Liverpool. In 2009, he joined Tsinghua University as a Professor of Electrical Engineering and an Assistant President and the Deputy Director of the Laboratory of Low-Carbon Energy. During 2012 to 2017, he worked as the Executive Vice President of Zhejiang University, as well as Founding Dean of the International Campus and Professor of Electrical Engineering and Higher Education of the University. Since 2018, he became Rector of the University of Macau. His current research interests include smart grid, electricity economics, and operation and control of power systems.

Prof. Song was the recipient of the D.Sc. Award by Brunel University, in 2002, for his original achievements in power system research. He was elected as the Vice-President of Chinese Society for Electrical Engineering (CSEE) and appointed as the Chairman of the International Affairs Committee of the CSEE in 2009. In 2004, he was elected as a Fellow of the Royal Academy of Engineering, U.K.